Pseudo-Goldstone Modes and Dynamical Gap Generation from Order by Thermal Disorder

Subhankar Khatua[1,2,*] Michel J. P. Gingras[2] and Jeffrey G. Rau[1]

[1]*Department of Physics, University of Windsor, 401 Sunset Avenue, Windsor, Ontario N9B 3P4, Canada*
[2]*Department of Physics and Astronomy, University of Waterloo, Waterloo, Ontario N2L 3G1, Canada*

Accidental ground state degeneracies—those not a consequence of global symmetries of the Hamiltonian—are inevitably lifted by fluctuations, often leading to long-range order, a phenomenon known as "order-by-disorder" (ObD). The detection and characterization of ObD in real materials currently lacks clear, qualitative signatures that distinguish ObD from conventional energetic selection. We show that for order by *thermal* disorder (ObTD) such a signature exists: a characteristic temperature dependence of the fluctuation-induced pseudo-Goldstone gap. We demonstrate this in a minimal two-dimensional model that exhibits ObTD, the ferromagnetic Heisenberg-compass model on a square lattice. Using spin-dynamics simulations and self-consistent mean-field calculations, we determine the pseudo-Goldstone gap, Δ, and show that at low temperatures it scales as the square root of temperature, $\sqrt{T}$. We establish that a power-law temperature dependence of the gap is a general consequence of ObTD, showing that all key features of this physics can be captured in a simple model of a particle moving in an effective potential generated by the fluctuation-induced free energy.

Strongly competing interactions, or frustration, enhance quantum and thermal fluctuations, and undermine the development of conventional magnetic order. The latter can even be prevented entirely down to zero temperature, leading to classical [1–3] or quantum spin liquids [4–10]. However, additional perturbative interactions can relieve the frustration and favor the development of long-range order (LRO). Accordingly, the majority of spin liquid candidates ultimately evade fate as a spin liquid [8,11]. The ability of such perturbative interactions, largely inconsequential without frustration, to dictate the ground state and low-temperature properties of a system is at the root of the plethora of exotic phenomena displayed by highly frustrated magnetic materials [10,12–18].

This relief of frustration is not always complete. Instead of an extensively degenerate manifold, a system can possess a subextensive *accidental* ground state degeneracy, unprotected by symmetry. Classically, this degeneracy can be robust to a range of realistic interactions including symmetry-allowed two-spin exchange [19]. Here, the role of fluctuations is dramatically changed: instead of being detrimental, they can lift the classical degeneracy and stabilize order—this is the celebrated phenomenon of *order-by-disorder* (ObD) [20–22]. While numerous theoretical models have been proposed [20–33], there is a paucity of real materials that unambiguously harbor ObD [19,34–37]. The standard strategy for experimental confirmation of ObD is indirect, relying on parametrizing a theoretical model of the material, establishing ObD within

that model, and then validating its predictions for the ordered state experimentally.

While this program has been applied somewhat successfully to a handful of materials [19,34–37], the inability to evince ObD directly, without relying on detailed modeling, highlights something lacking in our understanding of ObD. Clear, *qualitative*, and model-independent signatures are needed; for example, experimental observation of characteristic power laws in heat capacity or transport can diagnose the character of low-energy excitations, such as exchange statistics, dimensionality, or their dispersion relations [9,11,38,39]. Does the presence of ObD exhibit a "smoking-gun" experimental signature? This can be difficult or subtle to discern. For ObD from quantum fluctuations [21], the formation of an ObD spin-wave gap is generally not distinguishable from one induced energetically by multispin interactions [40–42].

In this Letter, we identify a clear signature of order by *thermal* disorder (ObTD): a dynamically generated gap growing as the square root of temperature. We investigate this gapped "pseudo-Goldstone" (PG) mode [43–45] in a minimal 2D classical spin model exhibiting ObTD, the ferromagnetic Heisenberg-compass model on a square lattice, belonging to a class of models relevant to Mott insulators with strong spin-orbit coupling [46–54]. Through spin-dynamics simulations, we determine the PG gap Δ and show it varies with temperature as $\Delta \propto \sqrt{T}$, in quantitative agreement with the self-consistent mean-field theory (SCMFT) that we present. This mode is well

defined, with its linewidth Γ due to thermal broadening, $\Gamma \propto T^2 \ll \Delta$. We further demonstrate that our key results can be captured by an effective description of a particle moving in a potential generated by the fluctuation-induced free energy. Using this picture, we argue that the temperature dependence of the PG gap, $\sqrt{T}$ (T) for type-I (II) PG modes, which have dispersion $\omega \propto |\mathbf{k}|$ and $\omega \propto |\mathbf{k}|^2$, respectively [55], is *universal* and applicable to *any* system exhibiting ObTD. Finally, due to the low dimensionality [56] of the 2D model considered, ObTD faces a subtle competition against potentially infrared-divergent fluctuations [57,58]. While ObTD ultimately prevails and true LRO develops, the magnetization displays logarithmic corrections at low temperatures, a remnant of the diverging infrared fluctuations.

Model.—We consider the *classical* ferromagnetic Heisenberg-compass model on a square lattice

$$\mathcal{H} = \sum_{\mathbf{r}} \left[-J \sum_{\delta=x,y} \mathbf{S}_{\mathbf{r}} \cdot \mathbf{S}_{\mathbf{r}+\delta} - K(S_{\mathbf{r}}^x S_{\mathbf{r}+x}^x + S_{\mathbf{r}}^y S_{\mathbf{r}+y}^y) \right], \quad (1)$$

where $\mathbf{S}_{\mathbf{r}} \equiv (S_{\mathbf{r}}^x, S_{\mathbf{r}}^y, S_{\mathbf{r}}^z)$ is a unit vector at site $\mathbf{r}$, and $\delta = x, y$ denote the nearest-neighbor bonds. We consider ferromagnetic Heisenberg and compass interactions with $J > 0$, $K > 0$ [see Supplemental Material (SM) [59] for a discussion of other signs] and with J the unit of energy, setting $J \equiv \hbar \equiv k_B \equiv 1$ throughout.

For $K = 0$, the model [Eq. (1)] is the well-known Heisenberg ferromagnet with uniform ferromagnetic ground states of arbitrary direction, $\mathbf{S}_{\mathbf{r}} = \hat{\mathbf{n}}$, related by global spin-rotation symmetry. For $K > 0$, this symmetry is absent and $\mathcal{H}$ in Eq. (1) is minimized by any uniform magnetization in the $\hat{\mathbf{x}}$-$\hat{\mathbf{y}}$ plane. These ground states are characterized by an angle $\phi \in [0, 2\pi)$ with $\mathbf{S}_{\mathbf{r}} = \cos\phi \,\hat{\mathbf{x}} + \sin\phi \,\hat{\mathbf{y}}$. Unlike the pure Heisenberg ferromagnet, these are only *accidentally* degenerate, as continuous in-plane spin rotations do not preserve the anisotropic compass term. However, a discrete C_4 symmetry about the $\hat{\mathbf{z}}$ axis and C_2 symmetries about the $\hat{\mathbf{x}}$ and $\hat{\mathbf{y}}$ axes still remain.

Simulations.—We first demonstrate that this model exhibits ObTD via Monte Carlo (MC) simulations on a lattice with $N = L^2$ sites. To expose the state selection, we construct a probability distribution for the magnetization orientation ϕ, $P(\phi)$, using a sample of thermalized states (see SM [59]). As shown in Fig. 1(a), $P(\phi)$ exhibits maxima at $\phi = 0$, $\pi/2$, π, $3\pi/2$, corresponding to ferromagnetic ground states with $\hat{\mathbf{n}}$ along the $\pm\hat{\mathbf{x}}$, $\pm\hat{\mathbf{y}}$ directions. At low temperatures, fluctuations thus select four discrete ground states via ObTD from a one-parameter manifold of states.

We now consider the classical dynamics to examine the associated PG mode. The equation of motion for the classical spins is the Landau-Lifshitz equation [76],

$d\mathbf{S}_{\mathbf{r}}/dt = \mathbf{B}_{\mathbf{r}} \times \mathbf{S}_{\mathbf{r}}$, describing precession about the exchange field $\mathbf{B}_{\mathbf{r}}$ produced by neighboring spins

$$\mathbf{B}_{\mathbf{r}} \equiv - \sum_{\delta=\pm x,\pm y} [J\mathbf{S}_{\mathbf{r}+\delta} + K S_{\mathbf{r}+\delta}^\delta \delta]. \quad (2)$$

Starting with states drawn via MC sampling at temperature T, we numerically integrate the Landau-Lifshitz equations, and compute the dynamical structure factor, $\mathcal{S}(\mathbf{k}, \omega) = \langle |\mathbf{S}_{\mathbf{k}}(\omega)|^2 \rangle$, where $\mathbf{S}_{\mathbf{k}}(\omega)$ is the Fourier transform of the spins, and $\langle \cdots \rangle$ denotes averaging over the initial states [59]. Results for $\mathcal{S}(\mathbf{k}, \omega)$ at a representative T and K [59] are shown in Fig. 1(b), exhibiting sharp spin waves with a *nearly* gapless mode at $\mathbf{k} = \mathbf{0}$. Closer examination reveals a well-defined gap, as highlighted in the top right inset of Fig. 1(b)—this is the PG gap.

To determine the PG gap *quantitatively*, we consider a cut of the structure factor at $\mathbf{k} = \mathbf{0}$, i.e., $\mathcal{S}(\mathbf{0}, \omega)$. As the PG gap is much smaller than the bandwidth of the spectrum [see Fig. 1(b)], a significantly higher frequency resolution is required to accurately compute the gap [59], so a much longer integration time window is necessary. Cuts, $\mathcal{S}(\mathbf{0}, \omega)$, for several temperatures are presented in Fig. 1(c), with the peak location indicating the PG gap (see SM [59]). The temperature dependence of Δ is shown in Fig. 2. The leading contribution to the PG gap scales as the *square root* of temperature, vanishing as $T \to 0$, being well described by the fit $\Delta \sim 2.46\sqrt{T}$.

The thermal broadening of the spectrum induces a finite width to all excitations, including the PG mode. The PG mode linewidth, Γ, can be obtained from the full-width at half maximum of $\mathcal{S}(\mathbf{0}, \omega)$ [see Fig. 1(c)] as a function of temperature. The inset in Fig. 2 shows that $\Gamma \propto T^2$ at low temperatures (see SM [59]). Since $\Gamma \ll \Delta$ as $T \to 0$, this PG mode is well defined.

Spin-wave analysis.—The simulations reveal that the system displays LRO and hosts a PG excitation, where the PG gap and linewidth scale with temperature as $\sqrt{T}$ and T^2, respectively. To understand how these scaling laws arise, we consider a spin-wave analysis about the ordered state [60]. Since tackling spin-wave interactions is difficult within a purely classical approach [77–79], we follow the more widely used and computationally convenient quantum spin-wave analysis [61,62,80], taking the classical limit only at the end.

We first discuss the spectrum and state selection due to ObTD in linear spin-wave theory (LSWT). Expanding about a classical ground state (parametrized by ϕ) using the Holstein-Primakoff (HP) transformation [60], we obtain to $O(S)$

$$\mathcal{H}_2 = \sum_{\mathbf{k}} \left[A_{\mathbf{k}} a_{\mathbf{k}}^\dagger a_{\mathbf{k}} + \frac{1}{2!}(B_{\mathbf{k}} a_{\mathbf{k}}^\dagger a_{-\mathbf{k}}^\dagger + \text{H.c.}) \right], \quad (3)$$

where $a_{\mathbf{k}}$ denotes the bosonic annihilation operator at wave vector $\mathbf{k}$, and $A_{\mathbf{k}}$ and $B_{\mathbf{k}}$ depend on ϕ, J, and K
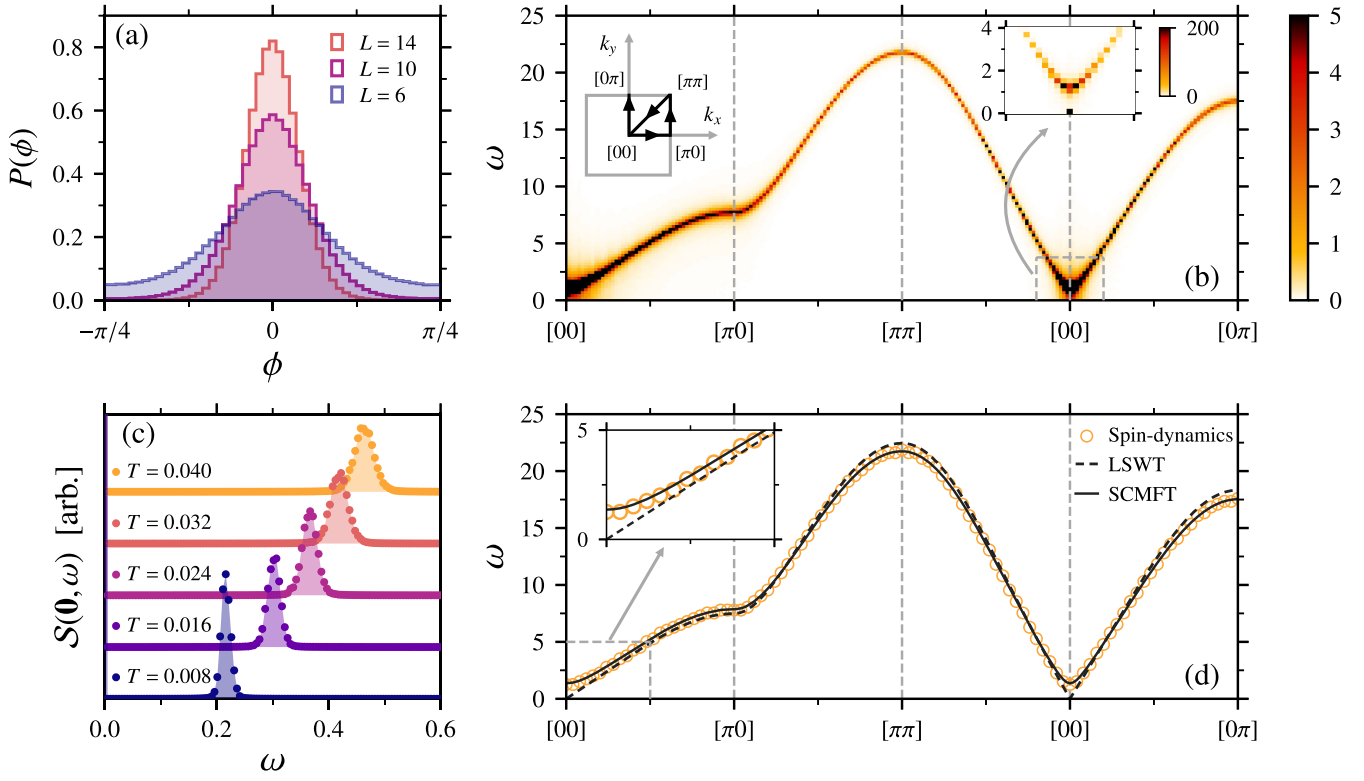
FIG. 1.   (a) Probability distribution, $P(\phi)$, of the angle, ϕ, characterizing the direction of the net magnetization obtained using MC simulations with $K = 5$ at $T = 0.4$ for several system sizes L. Because of C_4 symmetry, $P(\phi)$ is shown for $\phi \in [-\pi/4, \pi/4]$. (b) Dynamical structure factor, $\mathcal{S}(\boldsymbol{k}, \omega)$ obtained from spin-dynamics simulations for $L = 100$ with $K = 5$ at $T = 0.4$ along a path through the Brillouin zone (see left inset). The overall intensity is arbitrary. (Right inset) Spectrum near [00] showing the PG gap [75]. (c) Dynamical structure factor at $\boldsymbol{k} = \boldsymbol{0}$, $\mathcal{S}(\boldsymbol{0}, \omega)$, obtained from spin-dynamics simulations for $L = 40$ at various temperatures with $K = 5$. As above, the overall intensity is arbitrary. (d) Excitation spectrum along the same path as in panel (b) from the LSWT, SCMFT, and spin-dynamics simulations with $K = 5$ for $L = 100$ at $T = 0.4$. The spin-dynamics spectrum tracks the frequencies of maximum of $\mathcal{S}(\boldsymbol{k}, \omega)$. The inset highlights a small region near [00], showing the PG mode.

(see SM [59]). $\mathcal{H}_2$ in Eq. (3) can be diagonalized by a Bogoliubov transformation [60], giving spin-wave energies $\omega_{\boldsymbol{k}} = \sqrt{A_{\boldsymbol{k}}^2 - B_{\boldsymbol{k}}^2}$. As the spectrum depends on the ground state angle ϕ, fluctuations can lift the accidental classical degeneracy. To examine state selection due to ObTD, we search for the ground states for which the free energy is minimal. Starting with the quantum free energy $F_{\mathrm{Q}} = \frac{1}{2}\sum_{\boldsymbol{k}}\omega_{\boldsymbol{k}} + T\sum_{\boldsymbol{k}} \ln\left(1 - e^{-\omega_{\boldsymbol{k}}/T}\right)$, the classical limit, $T \gg \omega_{\boldsymbol{k}}$ yields $F_{\mathrm{Q}} \to F = T\sum_{\boldsymbol{k}} \ln \omega_{\boldsymbol{k}}$ [81]. This classical free energy has four minima at $\phi = 0$, $\pi/2$, π, $3\pi/2$—establishing selection by ObTD, in agreement with the MC results.

Within LSWT, quantum and classical calculations give the same spectrum, $\omega_{\boldsymbol{k}}$ [22]. This spectrum, calculated about $\phi = 0$, exhibits a gapless mode at $\boldsymbol{k} = \boldsymbol{0}$ as shown in Fig. 1(d). To obtain a PG gap, spin-wave interactions must be included, as we next discuss.

Interacting spin waves.—Performing the HP expansion to next order in $1/S$, the LSWT Hamiltonian [Eq. (3)] is augmented by interaction terms. Three-boson interactions are absent due to a C_2 symmetry about the ordering

direction, leaving only terms quartic in the bosons at $O(S^0)$ (see SM [59]). To treat this interacting problem, we adopt a mean-field approach [61,62], decoupling the quartic terms into products of quadratic terms and thermal averages of two-boson operators. Following this procedure, the new effective quadratic Hamiltonian mirrors Eq. (3), but with $A_{\boldsymbol{k}}$ and $B_{\boldsymbol{k}}$ replaced with $(A_{\boldsymbol{k}} + \delta A_{\boldsymbol{k}})$ and $(B_{\boldsymbol{k}} + \delta B_{\boldsymbol{k}})$. These corrections are

$$\delta A_{\boldsymbol{k}} = \frac{1}{N}\sum_{\boldsymbol{q}}\left[V_{\boldsymbol{k},\boldsymbol{q},\boldsymbol{0}}\langle a_{\boldsymbol{q}}^{\dagger}a_{\boldsymbol{q}}\rangle + \frac{1}{2}\left(D_{\boldsymbol{q},-\boldsymbol{q},\boldsymbol{k}}\langle a_{\boldsymbol{q}}^{\dagger}a_{-\boldsymbol{q}}^{\dagger}\rangle + \text{c.c.}\right)\right],$$

$$\delta B_{\boldsymbol{k}} = \frac{1}{N}\sum_{\boldsymbol{q}}\left[D_{\boldsymbol{k},-\boldsymbol{k},\boldsymbol{q}}\langle a_{\boldsymbol{q}}^{\dagger}a_{\boldsymbol{q}}\rangle + \frac{1}{2}V_{\boldsymbol{q},-\boldsymbol{q},\boldsymbol{k}-\boldsymbol{q}}\langle a_{\boldsymbol{q}}a_{-\boldsymbol{q}}\rangle\right], \quad (4)$$

where $V_{\boldsymbol{k}_1,\boldsymbol{k}_2,\boldsymbol{k}_3}$ and $D_{\boldsymbol{k}_1,\boldsymbol{k}_2,\boldsymbol{k}_3}$ are the coefficients for the 2-2 and 3–1 magnon scattering terms at $O(S^0)$ [59], and $\langle \cdots \rangle$ is a thermal average. When these averages are computed using LSWT [Eq. (3)], the corrections [Eq. (4)] reproduce the results obtained from leading order perturbation
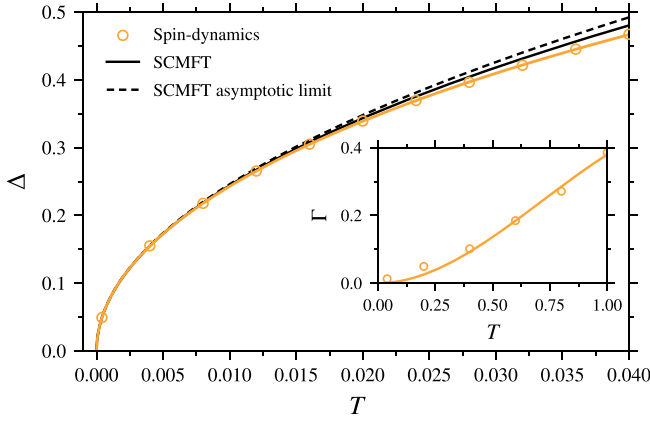
FIG. 2. Pseudo-Goldstone gap, Δ, as a function of temperature from spin-dynamics simulations with $K = 5$. The data are well described by the fit $\Delta = 2.462\,42\sqrt{T} - 3.219\,07\,T^{3/2}$. The SCMFT gap agrees with it quantitatively and provides the asymptotic $T \to 0$ scaling, $2.461\,47\sqrt{T}$. The asymptotic limit of the SCMFT gap is obtained from a calculation at a fixed low temperature $T = 0.001$. Inset: linewidth of the PG mode, Γ, as a function of temperature from spin-dynamics simulations. It is well described by the fit, $\Gamma = 0.709\,286\,T^2 - 0.329\,751\,T^3$. All data have been extrapolated in the system size to the thermodynamic limit [59].

theory [63,64]. However, because of the gapless mode, these δA_k and δB_k individually diverge in the ($T \gg \omega_k$) classical limit and perturbation theory breaks down [59].

To resolve these divergences, we compute the averages in Eq. (4) using SCMFT, obtaining a renormalized spectrum Ω_k (see SM [59]). Explicitly, $\langle a_k^\dagger a_k \rangle$ and $\langle a_k a_{-k} \rangle$ are, classically, computed self-consistently (until convergence) using Eq. (4) and

$$\langle a_k^\dagger a_k \rangle = \frac{T(A_k + \delta A_k)}{\Omega_k^2}, \quad \langle a_k a_{-k} \rangle = -\frac{T(B_k + \delta B_k)}{\Omega_k^2}, \quad (5)$$

where $\Omega_k = \sqrt{(A_k + \delta A_k)^2 - (B_k + \delta B_k)^2}$ and $\langle a_k a_{-k} \rangle = \langle a_k^\dagger a_{-k}^\dagger \rangle$.

The SCMFT spectrum Ω_k, plotted in Fig. 1(d), exhibits a clear gap at $k = 0$. The PG mode, gapless in LSWT, has now become gapped due to magnon-magnon interactions. Excellent agreement between the spectra from SCMFT and spin-dynamics simulations is observed across the full Brillouin zone [see Fig. 1(d)]. The temperature dependences of Δ from these two approaches in Fig. 2 agree quantitatively, with the same $\sqrt{T}$ scaling as $T \to 0$. This is a key result of this Letter, establishing a clear spectral *signature* of ObTD.

While the SCMFT is successful in describing the excitation energies, it does not address thermal broadening, since δA_k and δB_k are real, giving an infinite magnon lifetime. To obtain a finite linewidth, perturbation theory must be carried out to higher order. We expect that $\delta A_0 \equiv \delta A_{k=0}$ and $\delta B_0 \equiv \delta B_{k=0}$, interpreted as contributions

to the magnon self-energy [59], can be expanded in T as $\delta A_0 = a_1 T + a_2 T^2 + \cdots$ and $\delta B_0 = b_1 T + b_2 T^2 + \cdots$. Since $|A_0| = |B_0|$, reflecting the gapless LSWT spectrum, and a_1, b_1 [the $O(T)$ corrections in Eq. (4)] are real; any imaginary part, and thus finite lifetime, must arise from a_2 or b_2. Expanding $\Omega_0 \equiv \Omega_{k=0}$ in T yields $\mathrm{Im}\,\Omega_0 \approx (\mathrm{Im}\,a_2)T^2 + \cdots$ (see SM [59]). The real part, $\mathrm{Re}\,\Omega_0$, maintains its leading $\sqrt{T}$ dependence (providing the PG gap) while $\mathrm{Im}\,\Omega_0$, giving the linewidth, displays a leading T^2 dependence, consistent with the simulation results (see inset of Fig. 2).

Effective description.—We now present an effective description capturing the key aspects of the PG mode in a significantly simpler language and with broader applicability, adapting an approach previously formulated for order by quantum disorder (ObQD) [65]. We consider small uniform deviations (i.e., at $k = 0$) from a classical ground state (say $\phi = 0$) with $S_r \approx (\sqrt{1 - \phi^2 - \theta^2}, \phi, \theta)$, accurate to quadratic order in ϕ and θ, where ϕ is the soft mode and θ its conjugate momentum. For small ϕ and θ, $\phi \approx (1/N) \sum_r S_r^y$ and $\theta \approx (1/N) \sum_r S_r^z$, with Poisson bracket $\{\phi, \theta\} = 1/N$, obtained from the canonical relation $\{S_r^y, S_{r'}^z\} = \delta_{r,r'} S_r^x \approx \delta_{r,r'}$ (taking $S_r^x \approx 1$ as $\hat{x}$ is the ordered moment direction). For this configuration, we define an effective free energy $F_{\mathrm{eff}}(\theta, \phi) = E_{\mathrm{cl}}(\theta) - TS(\phi)$, where $E_{\mathrm{cl}}(\theta)$ is the classical energy cost of nonzero θ and $S(\phi) = -\sum_k \ln \omega_k(\phi)$ is the entropy. For small θ and ϕ, F_{eff} can be expanded as $F_{\mathrm{eff}} \approx \frac{1}{2} N(C_\theta \theta^2 + C_\phi \phi^2)$, where $C_\theta = (\partial^2 F_{\mathrm{eff}}/\partial\theta^2)/N = 2K$ and $C_\phi = (\partial^2 F_{\mathrm{eff}}/\partial\phi^2)/N$. Taking F_{eff} as an effective Hamiltonian, the equations of motion [82] for θ and ϕ are

$$\frac{\partial\phi}{\partial t} = +\frac{1}{N}\frac{\partial F_{\mathrm{eff}}}{\partial\theta} = +C_\theta\theta, \quad \frac{\partial\theta}{\partial t} = -\frac{1}{N}\frac{\partial F_{\mathrm{eff}}}{\partial\phi} = -C_\phi\phi, \quad (6)$$

describing a harmonic oscillator. We identify the PG gap as its frequency, $\Delta = \sqrt{C_\theta C_\phi}$. Remarkably, the $\sqrt{T}$ dependence of the PG gap is recovered, since C_ϕ is $O(T)$ and C_θ is $O(1)$. The curvature C_ϕ can be calculated from $-TS(\phi)$ within LSWT, yielding a frequency $2.461\,47\sqrt{T}$ for $K = 5$—exactly the PG gap found in SCMFT as $T \to 0$ and in agreement with the spin-dynamics simulations (see Fig. 2).

While formulated for the Heisenberg-compass model, this line of argument can be deployed to obtain the PG gap for *any* spin model exhibiting ObTD. A proof of this statement, following the strategy of Ref. [65], will be reported elsewhere [83]. For type-I PG modes ($\omega \propto |k|$, as in the Heisenberg-compass model we consider here), C_θ is T independent and $C_\phi \sim O(T)$, giving $\Delta \propto \sqrt{T}$. For type-II PG modes ($\omega \propto |k|^2$, e.g., in the ferromagnetic Heisenberg-compass model on the *cubic* lattice [65]), both θ and ϕ are soft modes with both thus giving entropic contributions to
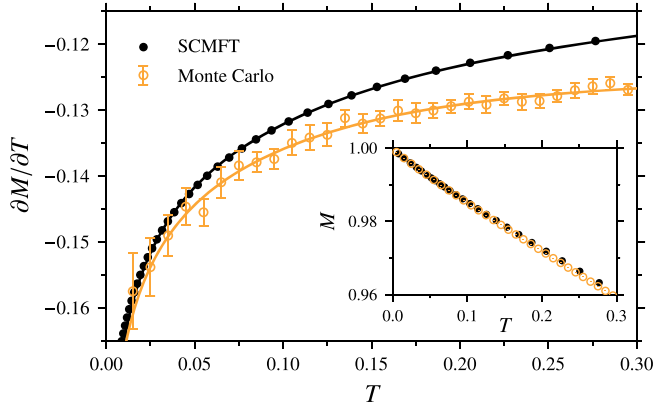
FIG. 3. Derivative of magnetization with respect to temperature, $\partial M/\partial T$, as a function of temperature for $L = 60$, $K = 5$ using MC simulation and SCMFT. MC data are well described by a fit motivated by SCMFT [59], $-0.09815 - 0.03563T + 0.01485 \ln T$. A similar fit to SCMFT data yields $-0.09631 - 0.01494T + 0.01491 \ln T$. The inset shows M as a function of temperature for the same parameters. MC error bars on M are smaller than the symbol size.

the free energy, leading to $C_\theta \sim O(T)$, $C_\phi \sim O(T)$ and thus $\Delta \propto T$.

Consequences of quasi-infrared-divergent fluctuations.— The ability to obtain the PG gap from LSWT presents a puzzle: the perturbative corrections δA_0 and δB_0 diverge logarithmically with system size [56], just as in the Mermin-Wagner-Hohenberg theorem [57,58]. How then do the curvatures of F_{eff} avoid these singularities and give the correct scaling? An analysis of the infrared divergences [59] shows that while δA_0 and δB_0 are each singular, $\delta A_0 + \delta B_0$, which determines the leading contribution to the PG gap, is *finite* and reproduces the result from Eq. (6). However, divergences in higher order terms do not cancel, and must be cured self-consistently [59].

While the divergences are mostly benign within perturbation theory for the PG gap calculations, they appear more dramatically in other quantities [84], like the magnetization, $M = 1 - (1/N) \sum_k \langle a_k^\dagger a_k \rangle$. Here, the thermal population, $\langle a_k^\dagger a_k \rangle$ diverges in LSWT, rendering SCMFT necessary to obtain meaningful results. In SCMFT, the PG gap provides an infrared cutoff $\ell \sim 1/\Delta \propto 1/\sqrt{T}$, giving a logarithmic contribution to M scaling as $\propto T \ln T$ as $T \to 0$ [59]. The presence of this term can be diagnosed from $\partial M/\partial T$, which exhibits a logarithmic singularity as $T \to 0$ for both the MC simulations and SCMFT (see Fig. 3).

Outlook.—Our analysis of the PG gap will provide a deeper understanding of real materials exhibiting ObD. The existence of PG modes has been used to diagnose ObD, for example in the compounds $Fe_2Ca_3(GeO_4)_3$ [34], $Sr_2Cu_3O_4Cl_2$ [35], and $Er_2Ti_2O_7$ [36,41,85]. In such materials, the ObQD gap likely dominates the ObTD-induced gap discussed in this Letter. However, in systems

where the effect of ObQD is weak or the degrees of freedom are sufficiently classical, ObTD can resurface as the leading selection effect. For example, our results may shed light on the rapidly growing family of two-dimensional van der Waals (vdW) ferromagnets [86–88] where the ObQD gap is expected to be small and thus the contribution to the gap caused by thermal fluctuations may be more significant. Additionally, while reaching the classical (ObTD) selection regime is challenging in magnetic materials (due to small spin length S), it may be more accessible in other platforms such as those involving lattice vibrations [89,90], dipole-coupled nanoconfined molecular rotors [91–94] or artificial mesoscale magnetic crystals [95–98]. Whether ObTD can be realized in such topical systems, and how to detect the temperature dependent PG gap, are open questions. Our approach provides a theoretical framework and guidance for future experimental studies in this promising area of research.

---

[*]Corresponding author.
skhatua1@uwaterloo.ca

[1] P. W. Anderson, Ordering and antiferromagnetism in ferrites, Phys. Rev. **102**, 1008 (1956).

[2] Jacques Villain, Insulating spin glasses, Z. Phys. B **33**, 31 (1979).

[3] R. Moessner and J. T. Chalker, Low-temperature properties of classical geometrically frustrated antiferromagnets, Phys. Rev. B **58**, 12049 (1998).

[4] B. Canals and C. Lacroix, Pyrochlore Antiferromagnet: A Three-Dimensional Quantum Spin Liquid, Phys. Rev. Lett. **80**, 2933 (1998).

[5] Alexei Kitaev, Anyons in an exactly solved model and beyond, Ann. Phys. (Amsterdam) **321**, 2 (2006).

[6] M. J. P. Gingras and P. A. McClarty, Quantum spin ice: A search for gapless quantum spin liquids in pyrochlore magnets, Rep. Prog. Phys. **77**, 056501 (2014).

[7] Lucile Savary and Leon Balents, Quantum spin liquids: A review, Rep. Prog. Phys. **80**, 016502 (2017).

[8] Takashi Imai and Young S. Lee, Do quantum spin liquids exist?, Phys. Today **69**, No. 8, 30 (2016).

[9] J. Knolle and R. Moessner, A field guide to spin liquids, Annu. Rev. Condens. Matter Phys. **10**, 451 (2019).

[10] Leon Balents, Spin liquids in frustrated magnets, Nature (London) **464**, 199 (2010).

[11] Jinsheng Wen, Shun-Li Yu, Shiyan Li, Weiqiang Yu, and Jian-Xin Li, Experimental identification of quantum spin liquids, npj Quantum Mater. **4**, 12 (2019).

[12] *Introduction to Frustrated Magnetism: Materials, Experiments, Theory,* edited by C. Lacroix, P. Mendels, and F. Mila (Springer, Berlin, 2011), 10.1007/978-3-642-10589-0.

[13] *Spin Ice,* edited by M. Udagawa and L. Jaubert (Springer, Cham, 2021), 10.1007/978-3-030-70860-3.

[14] Jason S. Gardner, Michel J. P. Gingras, and John E. Greedan, Magnetic pyrochlore oxides, Rev. Mod. Phys. **82**, 53 (2010).

[15] Alannah M. Hallas, Jonathan Gaudet, and Bruce D. Gaulin, Experimental insights into ground-state selection of quantum XY pyrochlores, Annu. Rev. Condens. Matter Phys. **9**, 105 (2018).

[16] Jeffrey G. Rau and Michel J. P. Gingras, Frustrated quantum rare-earth pyrochlores, Annu. Rev. Condens. Matter Phys. **10**, 357 (2019).

[17] Simon Trebst and Ciarán Hickey, Kitaev materials, Phys. Rep. **950**, 1 (2022).

[18] H. Takagi, T. Takayama, G. Jackeli, G. Khaliullin, and S. E. Nagler, Concept and realization of Kitaev quantum spin liquids, Nat. Rev. Phys. **1**, 264 (2019).

[19] Lucile Savary, Kate A. Ross, Bruce D. Gaulin, Jacob P. C. Ruff, and Leon Balents, Order by Quantum Disorder in $Er_2Ti_2O_7$, Phys. Rev. Lett. **109**, 167201 (2012).

[20] J. Villain, R. Bidaux, J.-P. Carton, and R. Conte, Order as an effect of disorder, J. Phys. (Les Ulis, Fr.) **41**, 1263 (1980).

[21] E. F. Shender, Antiferromagnetic garnets with fluctuationally interacting sublattices, Zh. Eksp. Teor. Fiz. **83**, 326 (1982) [Sov. Phys. JETP **56**, 178 (1982)].

[22] Christopher L. Henley, Ordering due to Disorder in a Frustrated Vector Antiferromagnet, Phys. Rev. Lett. **62**, 2056 (1989).

[23] Jack R. Tessman, Magnetic anisotropy at $0\,°K$, Phys. Rev. **96**, 1192 (1954).

[24] Sona Prakash and Christopher L. Henley, Ordering due to disorder in dipolar magnets on two-dimensional lattices, Phys. Rev. B **42**, 6574 (1990).

[25] Kenn Kubo and Tatsuya Kishi, Ordering due to quantum fluctuations in the frustrated Heisenberg model, J. Phys. Soc. Jpn. **60**, 567 (1991).

[26] Andrey Chubukov, Order from Disorder in a Kagomé Antiferromagnet, Phys. Rev. Lett. **69**, 832 (1992).

[27] Jan N. Reimers and A. J. Berlinsky, Order by disorder in the classical Heisenberg kagomé antiferromagnet, Phys. Rev. B **48**, 9539 (1993).

[28] S. T. Bramwell, M. J. P. Gingras, and J. N. Reimers, Order by disorder in an anisotropic pyrochlore lattice antiferromagnet, J. Appl. Phys. **75**, 5523 (1994).

[29] Christopher L. Henley, Selection by Quantum Fluctuations of Dipolar Order in a Diamond Lattice, Phys. Rev. Lett. **73**, 2788 (1994).

[30] J. D. M. Champion, M. J. Harris, P. C. W. Holdsworth, A. S. Wills, G. Balakrishnan, S. T. Bramwell, E. Čižmár, T. Fennell, J. S. Gardner, J. Lago, D. F. McMorrow, M. Orendáč, A. Orendáčová, D. McK. Paul, R. I. Smith, M. T. F. Telling, and A. Wildes, $Er_2Ti_2O_7$: Evidence of quantum order by disorder in a frustrated antiferromagnet, Phys. Rev. B **68**, 020401(R) (2003).

[31] G. Baskaran, Diptiman Sen, and R. Shankar, Spin-S Kitaev model: Classical ground states, order from disorder, and exact correlation functions, Phys. Rev. B **78**, 115116 (2008).

[32] Paul A. McClarty, Pawel Stasiak, and Michel J. P. Gingras, Order-by-disorder in the XY pyrochlore antiferromagnet, Phys. Rev. B **89**, 024425 (2014).

[33] Bimla Danu, Gautam Nambiar, and R. Ganesh, Extended degeneracy and order by disorder in the square lattice J_1-J_2-J_3 model, Phys. Rev. B **94**, 094438 (2016).

[34] Th. Brueckel, B. Dorner, A. G. Gukasov, V. P. Plakhty, W. Prandl, E. F. Shender, and O. P. Smirnow, Dynamical interaction of antiferromagnetic subsystems: A neutron scattering study of the spinwave spectrum of the garnet $Fe_3Ca_3(GeO_4)_3$, Z. Phys. B **72**, 477 (1988).

[35] Y. J. Kim, A. Aharony, R. J. Birgeneau, F. C. Chou, O. Entin-Wohlman, R. W. Erwin, M. Greven, A. B. Harris, M. A. Kastner, I. Ya. Korenblit, Y. S. Lee, and G. Shirane, Ordering Due to Quantum Fluctuations in $Sr_2Cu_3O_4Cl_2$, Phys. Rev. Lett. **83**, 852 (1999).

[36] K. A. Ross, Y. Qiu, J. R. D. Copley, H. A. Dabkowska, and B. D. Gaulin, Order by Disorder Spin Wave Gap in the XY Pyrochlore Magnet $Er_2Ti_2O_7$, Phys. Rev. Lett. **112**, 057201 (2014).

[37] C. L. Sarkis, J. G. Rau, L. D. Sanjeewa, M. Powell, J. Kolis, J. Marbey, S. Hill, J. A. Rodriguez-Rivera, H. S. Nair, D. R. Yahne, S. Säubert, M. J. P. Gingras, and K. A. Ross, Unravelling competing microscopic interactions at a phase boundary: A single-crystal study of the metastable antiferromagnetic pyrochlore $Yb_2Ge_2O_7$, Phys. Rev. B **102**, 134418 (2020).

[38] N. W. Ashcroft and N. D. Mermin, *Solid State Physics* (Saunders College Publishing, Fort Worth, 1976).

[39] Xiao-Gang Wen, *Quantum Field Theory of Many-Body Systems: From the Origin of Sound to an Origin of Light and Electrons* (Oxford University Press, New York, 2007), https://academic.oup.com/book/25836?login=true.

[40] P. A. McClarty, S. H. Curnoe, and M. J. P. Gingras, Energetic selection of ordered states in a model of the $Er_2Ti_2O_7$ frustrated pyrochlore XY antiferromagnet, J. Phys. Conf. Ser. **145**, 012032 (2009).

[41] Sylvain Petit, Julien Robert, Solène Guitteny, Pierre Bonville, Claudia Decorse, Jacques Ollivier, Hannu Mutka, Michel J. P. Gingras, and Isabelle Mirebeau, Order by disorder or energetic selection of the ground state in the XY pyrochlore antiferromagnet $Er_2Ti_2O_7$: An inelastic neutron scattering study, Phys. Rev. B **90**, 060410(R) (2014).

[42] Jeffrey G. Rau, Sylvain Petit, and Michel J. P. Gingras, Order by virtual crystal field fluctuations in pyrochlore XY antiferromagnets, Phys. Rev. B **93**, 184408 (2016).

[43] Steven Weinberg, Approximate Symmetries and Pseudo-Goldstone Bosons, Phys. Rev. Lett. **29**, 1698 (1972).

[44] C. P. Burgess, Goldstone and pseudo-Goldstone bosons in nuclear, particle and condensed-matter physics, Phys. Rep. **330**, 193 (2000).

[45] Muneto Nitta and Daisuke A. Takahashi, Quasi-Nambu-Goldstone modes in nonrelativistic systems, Phys. Rev. D **91**, 025018 (2015).

[46] Zohar Nussinov and Jeroen van den Brink, Compass models: Theory and physical motivations, Rev. Mod. Phys. **87**, 1 (2015).

[47] Julien Dorier, Federico Becca, and Frédéric Mila, Quantum compass model on the square lattice, Phys. Rev. B **72**, 024448 (2005).

[48] G. Jackeli and G. Khaliullin, Mott Insulators in the Strong Spin-Orbit Coupling Limit: From Heisenberg to a Quantum Compass and Kitaev Models, Phys. Rev. Lett. 102, 017205 (2009).

[49] F. Trousselet, A. M. Oleś, and P. Horsch, Compass-Heisenberg model on the square lattice—spin order and elementary excitations, Europhys. Lett. 91, 40005 (2010).

[50] Fabien Trousselet, Andrzej M. Oleś, and Peter Horsch, Magnetic properties of nanoscale compass-Heisenberg planar clusters, Phys. Rev. B 86, 134412 (2012).

[51] S. Boseggia, R. Springell, H. C. Walker, H. M. Rønnow, Ch. Rüegg, H. Okabe, M. Isobe, R. S. Perry, S. P. Collins, and D. F. McMorrow, Robustness of Basal-Plane Antiferromagnetic Order and the $J_{\mathrm{eff}}=1/2$ State in Single-Layer Iridate Spin-Orbit Mott Insulators, Phys. Rev. Lett. 110, 117207 (2013).

[52] Vamshi M. Katukuri, Viktor Yushankhai, Liudmila Siurakshina, Jeroen van den Brink, Liviu Hozoi, and Ioannis Rousochatzakis, Mechanism of Basal-Plane Antiferromagnetism in the Spin-Orbit Driven Iridate Ba_2IrO_4, Phys. Rev. X 4, 021051 (2014).

[53] Artem A. Vladimirov, Dieter Ihle, and Nikolay M. Plakida, Magnetic order in the two-dimensional compass-Heisenberg model, Eur. Phys. J. B 88, 148 (2015).

[54] Long Zhang, Fa Wang, and Dung-Hai Lee, Compass impurity model of Tb substitution in Sr_2IrO_4, Phys. Rev. B 94, 161118(R) (2016).

[55] Haruki Watanabe, Counting rules of Nambu-Goldstone modes, Annu. Rev. Condens. Matter Phys. 11, 169 (2020).

[56] Sidney Coleman, There are no Goldstone bosons in two dimensions, Commun. Math. Phys. 31, 259 (1973).

[57] N. D. Mermin and H. Wagner, Absence of Ferromagnetism or Antiferromagnetism in One- or Two-Dimensional Isotropic Heisenberg Models, Phys. Rev. Lett. 17, 1133 (1966).

[58] P. C. Hohenberg, Existence of long-range order in one and two dimensions, Phys. Rev. 158, 383 (1967).

[59] See Supplemental Material at http://link.aps.org/supplemental/10.1103/PhysRevLett.130.266702 for details about Monte Carlo and spin-dynamics simulations and finite size scaling analysis, as well as details of the linear and nonlinear spin wave theory, including details of cancellation of divergences in the PG gap calculation and derivation of logarithmic correction to the magnetization. It also includes Refs. [60–74].

[60] A. Auerbach, Interacting Electrons and Quantum Magnetism, Graduate Texts in Contemporary Physics (Springer, New York, 1998), 10.1007/978-1-4612-0869-3.

[61] H. Bruus and K. Flensberg, Many-Body Quantum Theory in Condensed Matter Physics: An Introduction, Oxford Graduate Texts (Oxford University Press, Oxford, 2004).

[62] J. P. Blaizot and G. Ripka, Quantum Theory of Finite Systems (MIT Press, Cambridge, 1986).

[63] P. D. Loly, The Heisenberg ferromagnet in the selfconsistently renormalized spin wave approximation, J. Phys. C 4, 1365 (1971).

[64] A. V. Chubukov, S. Sachdev, and T. Senthil, Large-S expansion for quantum antiferromagnets on a triangular lattice, J. Phys. Condens. Matter 6, 8891 (1994).

[65] Jeffrey G. Rau, Paul A. McClarty, and Roderich Moessner, Pseudo-Goldstone Gaps and Order-By-Quantum Disorder in Frustrated Magnets, Phys. Rev. Lett. 121, 237201 (2018).

[66] J. D. Alzate-Cardona, D. Sabogal-Suárez, R. F. L. Evans, and E. Restrepo-Parra, Optimal phase space sampling for Monte Carlo simulations of Heisenberg spin systems, J. Phys. Condens. Matter 31, 095802 (2019).

[67] Michael Creutz, Overrelaxation and Monte Carlo simulation, Phys. Rev. D 36, 515 (1987).

[68] M. E. J. Newman and G. T. Barkema, Monte Carlo Methods in Statistical Physics (Clarendon Press, Oxford, 1999).

[69] J. R. Dormand and P. J. Prince, A family of embedded Runge-Kutta formulae, J. Comput. Appl. Math. 6, 19 (1980).

[70] K. Ahnert and M. Mulansky, Odeint—Solving ordinary differential equations in C++, AIP Conf. Proc. 1389, 1586 (2011).

[71] K. Ahnert and M. Mulansky, Boost C++ Library: Odeint (2012), https://www.boost.org/doc/libs/1_66_0/libs/numeric/odeint/doc/html/index.html.

[72] J. C. Bowman and M. Roberts, FFTW++: A fast Fourier transform C++ header class for the FFTW3 library (2010), https://fftwpp. sourceforge.net.

[73] M. E. Zhitomirsky and A. L. Chernyshev, Colloquium: Spontaneous magnon decays, Rev. Mod. Phys. 85, 219 (2013).

[74] P. M. Chaikin and T. C. Lubensky, Principles of Condensed Matter Physics (Cambridge University Press, Cambridge, England, 1995), 10.1017/CBO9780511813467.

[75] The lower intensity at the band minimum compared to its vicinity is a numerical artifact. Because of the finite frequency resolution of the spin-dynamics simulations, the intensity maximum of the PG mode may have fallen between frequency grid points, resulting in an (apparent) lower intensity at the band minimum.

[76] L. Landau and E. Lifshitz, 3—On the theory of the dispersion of magnetic permeability in ferromagnetic bodies, in Perspectives in Theoretical Physics, edited by L. P. Pitaevksi (Pergamon, Amsterdam, 1992), pp. 51–65 [reprinted from Phys. Z. Sowjetunion 8, Part 2, 153 (1935)], 10.1016/B978-0-08-036364-6.50008-9.

[77] P. C. Martin, E. D. Siggia, and H. A. Rose, Statistical dynamics of classical systems, Phys. Rev. A 8, 423 (1973).

[78] Uli Deker and Fritz Haake, Fluctuation-dissipation theorems for classical processes, Phys. Rev. A 11, 2043 (1975).

[79] C. P. Enz and L. Garrido, Perturbation theory for classical thermodynamic Green's functions, Phys. Rev. A 14, 1258 (1976).

[80] G. D. Mahan, Many Particle Physics, Third Edition (Springer, New York, 2000), 10.1007/978-1-4757-5714-9.

[81] Mehran Kardar, Statistical Physics of Particles (Cambridge University Press, Cambridge, England, 2007), 10.1017/CBO9780511815898.

[82] H. Goldstein, C. P. Poole, and J. L. Safko, Classical Mechanics, 3rd ed. (Pearson, Hoboken, New Jersey, 2002).

[83] Subhankar Khatua, Michel J. P. Gingras, and Jeffrey G. Rau (unpublished).

[84] P. A. Maksimov, Zhenyue Zhu, Steven R. White, and A. L. Chernyshev, Anisotropic-Exchange Magnets on a

Triangular Lattice: Spin Waves, Accidental Degeneracies, and Dual Spin Liquids, Phys. Rev. X **9**, 021017 (2019).

[85] E. Lhotel, J. Robert, E. Ressouche, F. Damay, I. Mirebeau, J. Ollivier, H. Mutka, P. Dalmas de Réotier, A. Yaouanc, C. Marin, C. Decorse, and S. Petit, Field-induced phase diagram of the *XY* pyrochlore antiferromagnet $Er_2Ti_2O_7$, Phys. Rev. B **95**, 134426 (2017).

[86] Cheng Gong, Lin Li, Zhenglu Li, Huiwen Ji, Alex Stern, Yang Xia, Ting Cao, Wei Bao, Chenzhe Wang, Yuan Wang, Z. Q. Qiu, R. J. Cava, Steven G. Louie, Jing Xia, and Xiang Zhang, Discovery of intrinsic ferromagnetism in two-dimensional van der Waals crystals, Nature (London) **546**, 265 (2017).

[87] Lebing Chen, Jae-Ho Chung, Matthew B. Stone, Alexander I. Kolesnikov, Barry Winn, V. Ovidiu Garlea, Douglas L. Abernathy, Bin Gao, Mathias Augustin, Elton J. G. Santos, and Pengcheng Dai, Magnetic Field Effect on Topological Spin Excitations in CrI_3, Phys. Rev. X **11**, 031047 (2021).

[88] S. E. Nikitin, B. Fåk, K. W. Krämer, T. Fennell, B. Normand, A. M. Läuchli, and Ch. Rüegg, Thermal Evolution of Dirac Magnons in the Honeycomb Ferromagnet $CrBr_3$, Phys. Rev. Lett. **129**, 127201 (2022).

[89] Yilong Han, Yair Shokef, Ahmed M. Alsayed, Peter Yunker, Tom C. Lubensky, and Arjun G. Yodh, Geometric frustration in buckled colloidal monolayers, Nature (London) **456**, 898 (2008).

[90] Yair Shokef, Anton Souslov, and T. C. Lubensky, Order by disorder in the antiferromagnetic Ising model on an elastic triangular lattice, Proc. Natl. Acad. Sci. U.S.A. **108**, 11804 (2011).

[91] Jerzy Cioslowski and Asiri Nanayakkara, Endohedral Fullerites: A New Class of Ferroelectric Materials, Phys. Rev. Lett. **69**, 2871 (1992).

[92] Shinobu Aoyagi, Norihisa Hoshino, Tomoyuki Akutagawa, Yuki Sado, Ryo Kitaura, Hisanori Shinohara, Kunihisa Sugimoto, Rui Zhang, and Yasujiro Murata, A cubic dipole lattice of water molecules trapped inside carbon cages, Chem. Commun. **50**, 524 (2014).

[93] B. P. Gorshunov, V. I. Torgashev, E. S. Zhukova, V. G. Thomas, M. A. Belyanchikov, C. Kadlec, F. Kadlec, M. Savinov, T. Ostapchuk, J. Petzelt, J. Prokleška, P. V. Tomas, E. V. Pestrjakov, D. A. Fursenko, G. S. Shakurov, A. S. Prokhorov, V. S. Gorelik, L. S. Kadyrov, V. V. Uskov, R. K. Kremer, and M. Dressel, Incipient ferroelectricity of water molecules confined to nano-channels of beryl, Nat. Commun. **7**, 12842 (2016).

[94] M. A. Belyanchikov *et al.*, Dielectric ordering of water molecules arranged in a dipolar lattice, Nat. Commun. **11**, 3927 (2020).

[95] Oleksandr V. Dobrovolskiy, Oleksandr V. Pylypovskyi, Luka Skoric, Amalio Fernández-Pacheco, Arjen Van Den Berg, Sam Ladak, and Michael Huth, Complex-shaped 3D nanoarchitectures for magnetism and superconductivity, in *Curvilinear Micromagnetism: From Fundamentals to Applications*, edited by Denys Makarov and Denis D. Sheka (Springer International Publishing, Cham, 2022), pp. 215–268, 10.1007/978-3-031-09086-8_5.

[96] Lukas Keller, Mohanad K. I. Al Mamoori, Jonathan Pieper, Christian Gspan, Irina Stockem, Christian Schröder, Sven Barth, Robert Winkler, Harald Plank, Merlin Pohlit, Jens Müller, and Michael Huth, Direct-write of free-form building blocks for artificial magnetic 3D lattices, Sci. Rep. **8**, 6160 (2018).

[97] Andrew May, Matthew Hunt, Arjen Van Den Berg, Alaa Hejazi, and Sam Ladak, Realisation of a frustrated 3D magnetic nanowire lattice, Commun. Phys. **2**, 13 (2019).

[98] Peter Fischer, Dédalo Sanz-Hernández, Robert Streubel, and Amalio Fernández-Pacheco, Launching a new dimension with 3D magnetic nanostructures, APL Mater. **8**, 010701 (2020).